

This is an electronic reprint of the original article. This reprint may differ from the original in pagination and typographic detail.

---

## Comparison of thermal decomposition and sequential dissolution - two sample preparation methods for radiocarbon dating of lime mortars

Daugbjerg, Thomas Schrøder; Lindroos, Alf; Hajdas, Irka; Ringbom, Åsa; Olsen, Jesper

*Published in:*  
Radiocarbon

*DOI:*  
[10.1017/RDC.2020.144](https://doi.org/10.1017/RDC.2020.144)

Published: 01/04/2021

*Document Version*  
(Peer reviewed version when applicable)

*Document License*  
CC BY-NC-ND

[Link to publication](#)

*Please cite the original version:*

Daugbjerg, T. S., Lindroos, A., Hajdas, I., Ringbom, Å., & Olsen, J. (2021). Comparison of thermal decomposition and sequential dissolution - two sample preparation methods for radiocarbon dating of lime mortars. *Radiocarbon*, 63(2), 405-427. <https://doi.org/10.1017/RDC.2020.144>

### General rights

Copyright and moral rights for the publications made accessible in the public portal are retained by the authors and/or other copyright owners and it is a condition of accessing publications that users recognise and abide by the legal requirements associated with these rights.

### Take down policy

If you believe that this document breaches copyright please contact us providing details, and we will remove access to the work immediately and investigate your claim.

1 **TITLE**

2

3 Comparison of thermal decomposition and sequential dissolution – Two sample preparation  
4 methods for radiocarbon dating of lime mortars

5

6 **AUTHORS**

7

8 Thomas Schröder Daugbjerg<sup>1,2</sup>, Alf Lindroos<sup>3</sup>, Irka Hajdas<sup>4</sup>, Åsa Ringbom<sup>5</sup>, Jesper Olsen<sup>1,2</sup>

9

10 **ADDRESSES**

11

12 <sup>1</sup>Aarhus AMS Centre (AARAMS), Department of Physics and Astronomy, Aarhus University,  
13 Aarhus, Denmark.

14 <sup>2</sup>Centre for Urban Network Evolutions (UrbNet), Aarhus University, Moesgård Allé 20, DK-8270  
15 Højbjerg

16 <sup>3</sup>Faculty of Science and Technology, Åbo Akademi University, Turku, Finland.

17 <sup>4</sup>Laboratory of Ion Beam Physics, ETH Zürich, Zürich, Switzerland

18 <sup>5</sup>Art History, Åbo Akademi University, Turku, Finland.

19

20 **CORRESPONDING AUTHOR**

21

22 Thomas Schröder Daugbjerg, Aarhus AMS Centre, Department of Physics and Astronomy, Aarhus  
23 University, Ny Munkegade 120, DK-8000 Aarhus C.

24 Email: [thomas.daugbjerg@phys.au.dk](mailto:thomas.daugbjerg@phys.au.dk)

25

26 **KEYWORDS**

27

28 Mortar dating, radiocarbon dating, sequential dissolution, thermal decomposition, preheating

29

30 **ABSTRACT**

31

32 Dating lime mortar samples using the radiocarbon method can be difficult. This is because the  
33 contamination is similar to the primary dating material ( $\text{CaCO}_3$ ) and consequently difficult to  
34 remove. Mortar can also have late-in-formation pyrogenic carbonate from interactions with the  
35 environment after the initial hardening phase, such as recrystallization, fire damage or delayed  
36 hardening. When radiocarbon dating a system of primary dating material, contamination and late-  
37 in-formation pyrogenic carbonate, one approach is multi-fraction dating with conclusiveness  
38 criteria. If a sample has sufficient contamination or late-in-formation pyrogenic carbonate, the  
39 criteria evaluate the result inconclusive. To improve inconclusive results from such samples, this  
40 study investigates sample preparation by thermal decomposition. Here samples that were  
41 inconclusively dated by the authors' traditional method, sequential dissolution with 85 %

42 phosphoric acid, are investigated further. This study finds that CO<sub>2</sub> thermally decomposed at low  
43 temperatures contains some late-in-formation pyrogenic carbonate. By rejecting CO<sub>2</sub> decomposed  
44 at low temperatures, Kastelholm castle and Kimito church in Finland are conclusively and  
45 accurately dated. Furthermore, a preheating method removes some late-in-formation carbonate, but  
46 not enough for a conclusive result. Finally, thermal decomposition finds difficulty in discerning  
47 binder carbonate from limestone and marble contamination.

48

## 49 **INTRODUCTION**

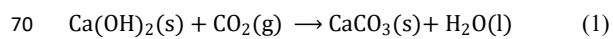
50

51 Radiocarbon dating of lime mortar is a method contributing to absolute dating in history and  
52 archaeology (Hale et al. 2003; Marzaioli et al. 2011; Ortega et al. 2012; Ringbom et al. 2014).  
53 Conclusive radiocarbon dating of a mortar sample determines the event of mortar hardening, which  
54 relates to the time of construction (Labeyrie and Delibrias 1964). For archaeological sites with  
55 mortared stone structures, mortar can be abundant and in a context that can be associated with the  
56 site's historical buildings (Heinemeier et al. 2010). Besides lime mortar, the presented radiocarbon  
57 methodologies are relevant for further anthropogenic carbonates such as ash, lime plaster and lime  
58 concrete (Toffolo et al. 2017; Toffolo et al. 2020). This study's samples are lime mortars, and the  
59 materials and methods section explains the selection of samples.

60 Production of lime mortar involves firing limestone, mainly made of calcite (CaCO<sub>3</sub>), at  
61 temperatures near or above 900 °C, where it thermally decomposes to form quicklime (CaO). The  
62 quicklime is slaked with water to produce slaked lime (Ca(OH)<sub>2</sub>). Finally, one mixes the slaked  
63 lime with an aggregate, typically sand, and wet mortar is ready to be applied as filling material  
64 between stones of the structure to be built. As wet mortar hardens, the contained slaked lime

65 consumes atmospheric CO<sub>2</sub> and binds it as CaCO<sub>3</sub>, see equation 1. In doing so, the CaCO<sub>3</sub> of lime  
66 mortar binder stores the atmospheric <sup>14</sup>C signal from the time of hardening, and this can  
67 potentially be radiocarbon dated (Labeyrie and Delibrias 1964; Stuiver and Smith 1965; Baxter and  
68 Walton 1970).

69



71

72 Radiocarbon dating of lime mortar has challenges such as geological carbonate, recrystallization,  
73 fire damage, delayed hardening and layered double hydroxide compounds (Labeyrie and Delibrias  
74 1964; Stuiver and Smith 1965; Baxter and Walton 1970; Sonninen and Jungner 1989; Heinemeier  
75 et al. 1997; Artioli et al. 2017; Ricci et al. 2020). Geological carbonate is several orders of  
76 magnitudes older than the <sup>14</sup>C half-life, and thus contains essentially no <sup>14</sup>C atoms. Contamination  
77 with geological carbonate can shift a mortar's <sup>14</sup>C concentration below the hardening's <sup>14</sup>C  
78 concentration. During production of mortar, the sand used as aggregate may contain grains of  
79 limestone, or limestone fragments may survive an incomplete burning of lime. In these ways, a  
80 mortar sample may have an inherent geological carbonate contamination. Recrystallization, fire  
81 damage, delayed hardening and layered double hydroxide compounds can shift a mortar's <sup>14</sup>C  
82 concentration above the hardening's <sup>14</sup>C concentration. In the presence of water, calcium carbonate  
83 is not entirely stable, and a mortar's binder may recrystallize and incorporate young CO<sub>2</sub> from the  
84 atmosphere. Fire damage may cause de-carbonation followed by re-activation of the binder and  
85 capture of new atmospheric CO<sub>2</sub> (Heinemeier et al. 2010; Lindroos et al. 2012). Delayed hardening  
86 can happen, if mortar has low permeability for CO<sub>2</sub> or if samples come from deeper parts in a  
87 construction. It introduces a delay between the time of construction and the time of hardening, and

88 it can leave unreacted calcium hydroxides (portlandite) so the sample is alkaline and absorbs  
89 modern CO<sub>2</sub> when sampled (Sonninen and Jungner 1989; Heinemeier et al. 1997; Michalska et al.  
90 2017). Layered double hydroxide (LDH) compounds can form from magnesium phases in dolomitic  
91 lime mortar and ancient hydraulic mortars such as pozzolana and cocchiopesto (Massazza 2003;  
92 Ponce-Anton et al. 2018; Ricci et al. 2020). LDHs can exchange carbonate anions with the  
93 atmosphere throughout the mortar's life and introduce young carbon dioxide (Artioli et al. 2017;  
94 Ponce-Anton et al. 2018; Ricci et al. 2020). This text uses the term, late-in-formation pyrogenic  
95 carbonate, to collectively refer to carbonate associated with recrystallization, fire damage, delayed  
96 hardening, alkalinity or LDHs.

97 Since the 1960's, the radiocarbon community has researched lime mortar as a material for  
98 radiocarbon dating (Labeyrie and Delibrias 1964; Stuiver and Smith 1965; Baxter and Walton 1970;  
99 Folk and Valastro 1976). In the 1990's and 2000's the sequential dissolution method develops, and  
100 it applies a single injection of 85% phosphoric acid to release the sample's carbonate as CO<sub>2</sub>.  
101 Extraction of CO<sub>2</sub> happens in multiple fractions throughout dissolution, and several fractions are  
102 radiocarbon dated by accelerator mass spectrometry (AMS) (Van Strydonck et al. 1986; Heinemeier  
103 et al. 1997; Ringbom et al. 2014). Sequential dissolution is explained further in the associated  
104 subsection in materials and methods. Here conclusive dating results follow from conclusiveness  
105 criteria that assert agreement among multiple CO<sub>2</sub> fractions (Heinemeier et al. 2010; Lindroos et al.  
106 2011; Ringbom et al. 2014). The discussion section describes conclusiveness criteria further.  
107 Heinemeier et al. (2010) compiled a successful study of lime mortars from the interior of Medieval  
108 churches. Here, 124 out of 150 samples were conclusive, and 75 out of 79 samples agreed with  
109 independent age control. There are other important approaches to radiocarbon dating of pyrogenic  
110 carbonates, and some are based on separation of a suitable dating fraction, e.g. by density  
111 separation, cryogenic-breaking, ultrasound, suspension, sedimentation or thermal treatment

112 (Marzaioli et al. 2011; Ortega et al. 2012; Toffolo et al. 2017; Ponce-Anton et al. 2018; Ricci et al.  
113 2020; Toffolo et al. 2020).

114 Mortar is a challenging material to radiocarbon date, and sequential dissolution and other  
115 preparation methods occasionally obtain inconclusive results, especially when the above challenges  
116 are abundant (Lichtenberger et al. 2015; Hajdas et al. 2017; Michalska et al. 2017; Ponce-Anton et  
117 al. 2018).

118 Recently, there has been an interest in sample preparation by thermal decomposition for pyrogenic  
119 calcium carbonate, such as ash or lime mortar (Toffolo et al. 2017; Ricci et al. 2020; Toffolo et al.  
120 2020). Thermal decomposition was actually the initial method used by Labeyrie and Delibrias  
121 (1964), but soon after acid hydrolysis became more prevalent (Stuiver and Smith 1965). The  
122 authors of this article have most often prepared mortar samples by sequential dissolution. Inspired  
123 by recent work, sample preparation by thermal decomposition revisits several challenging mortar  
124 samples. This contributes to methodological development of thermal decomposition as a  
125 preparation method for mortar dating. More broadly, it contributes to expanding the methods  
126 available to mortar dating, which may improve the conclusiveness when encountering the  
127 challenges described above. For example, sequential dissolution obtained inconclusive results for  
128 nearly all samples presented in this study, and this motivates other preparation methods.

129

## 130 **MATERIALS AND METHODS**

131

### 132 **Samples**

133

134 The samples come from Åbo Akademi's collection. There are three priorities when choosing  
135 samples. First, samples must have a known historical context such that results from sample  
136 preparation can be evaluated. The actual construction time is not known from historical sources, but  
137 previous dating has yielded ages that fit into the historical context, see Table 1. Second, samples  
138 must have one of the recurring challenges described in the introduction, so different preparation  
139 methodologies can investigate different challenges. Third and last, samples must have previous  
140 dating by sequential dissolution to compare with thermal decomposition.

141 To investigate geological carbonate's influence on  $^{14}\text{C}$  concentration in mortar this study presents  
142 mortar samples TTK005 and TTK006 from Turku cathedral in SW Finland and J13-ESM-1 from  
143 Jerash, Jordan.

144 The sample TTK006 comes from the pentagonal choir of Turku cathedral. Mortar dating was done  
145 in 2007, and results are presented in Lindroos et al. (2011; 2012; 2018). The sample was  
146 problematic because of abundant marble contamination, which may have masked other types of  
147 contamination. Sample TTK005, see Table 1, is from the same construction phase, and it has been  
148 dated in five  $\text{CO}_2$  fractions from the bulk mortar and three  $\text{CO}_2$  fractions from a lime lump within it  
149 (Lindroos et al. 2018). Sample TTK004 and TTK004Li are likewise a bulk mortar and a lime lump  
150 within it and taken close to sample TTK006. They were dated in 2017 in Zürich in 3  $\text{CO}_2$  fractions  
151 each (see Table 1), and the results have not been published earlier. The Pentagonal Choir is part of  
152 the original cathedral inaugurated in 1300 AD (Gardberg et al. 2000). It may have been renovated  
153 after destruction of the cathedral in 1318 AD (Gardberg et al. 2000; Lindroos et al. 2018).

154 The sample J13-ESM-1 comes from a water pipe cover in the ancient city Jerash, and Lichtenberger  
155 et al. (2015) discuss the sample further. Mortar dating with sequential dissolution was tried in 2015,  
156 and it proved difficult because of limestone aggregate. Lichtenberger et al. (2015) reports a charcoal



157 sample embedded in the mortar, usable for age control and radiocarbon dated to  $(1723\pm 25)$   $^{14}\text{C}$   
158 years BP.

159 To investigate the contribution to a mortar's  $^{14}\text{C}$  concentration from late-in-formation pyrogenic  
160 carbonate, this study presents mortar sample Kastel09 from Kastelholm castle in SW Finland, lime  
161 lump Kimito004Li from Kimito (Kemiö in Finnish) church in SW Finland and mortar sample  
162 Merida003 from Mérida amphitheater in W Spain.

163 Kastelholm is first mentioned in historical documents in 1388 AD (Hausen 1910). A trial to date the  
164 structurally oldest mortar with radiometric methods was made in 1985 (Sonninen and Jungner  
165 1989). Lindroos et al. (2020a) performed  $^{14}\text{C}$  dating prepared by sequential dissolution of sample  
166 Kastel09, and they present calendar date spans 1285-1312 AD with 41.5 % and 1359-1388 AD with  
167 53.9% probability. The age span 1285-1312 AD is interesting, because the nearby church of Jomala  
168 is from the 13<sup>th</sup> century AD (Ringbom et al. 2011). Other samples show late-in-formation pyrogenic  
169 carbonate either from alkalinity or fire damage. As an example of this sample Kastel10 is presented,  
170 which Lindroos et al. (2020a) also dated with sequential dissolution. We make thermal  
171 decomposition preparation of sample Kastel09, which is the least alkaline and has the least  
172 inhomogeneous  $\text{CO}_2$  fractions by sequential dissolution.

173 Sample Kimito004Li is a lime lump in a mortar from the attic of the sacristy in Kimito church, and  
174 it yielded an inconclusive result with sequential dissolution. On stylistic grounds, the famous mason  
175 *Petrus Murator* is considered the mason who vaulted the nave of Kimito church (Nikula 1975). It is  
176 documented that Petrus Murator was payed for finishing the vaulting of Turku cathedral in 1466  
177 AD (Hausen 1890; Nikula 1973), and the nave of Kimito church was most likely vaulted before  
178 1466 AD (Nikula 1975). Structurally, the sacristy is the oldest part of Kimito church, and it is  
179 stylistically attributed to the first half of the 15<sup>th</sup> century (Nikula 1975). Radiocarbon dating of

180 charred wood planks from the nave yielded variable ages from 889 AD to 1620 AD, see samples  
181 Kimito002W, Kimito003W and Kimito013W in Table 1. Furthermore, there are coin-finds from the  
182 early 14th century AD at Kimito church (Nikula 1975).

183 The Mérida Amphitheatre is either Augustan, early 1<sup>st</sup> century AD, or Flavian, late 1<sup>st</sup> century AD  
184 (Capello and Galán 1995; Mateos 2001). Mortar dating results from Mérida, including sample  
185 Merida003, have been published and suggest a late Flavian age (Hale et al. 2003; Ringbom et al.  
186 2006; Lindroos et al. 2020b). The Flavian dynasty spans from 69 AD to 96 AD (Jones et al. 2002).  
187 The Merida samples are very hard, have dolomitic chemistry, delayed hardening and shows  
188 abundant late-in-formation pyrogenic carbonates that dissolves before the binder carbonate  
189 (Lindroos et al. 2020b).

190

191 TableSamplesAndDates

192

### 193 **Sample pretreatment**

194

195 The sample pretreatment starts by gently crushing a sample with pliers (Heinemeier et al. 2010;  
196 Lichtenberger et al. 2015; Lindroos et al. 2018). The crushing is intentionally careful, i.e. not using  
197 too much force, as this can produce small grains of aggregate material, which may contain  
198 contaminating limestone (Heinemeier et al. 2010). Sieves with meshes from 100-500  $\mu\text{m}$  dry sieve  
199 the mortar into several grain size fractions (Van Strydonck et al. 1986). The dry sieving takes  
200 approximately 20 minutes using a mechanical sieve shaker, and the shaking promotes further  
201 crumbling of soft binder material. The grain size fraction  $<100 \mu\text{m}$  is wet sieved into several

202 fractions from <20  $\mu\text{m}$  to 100  $\mu\text{m}$ . According to Heinemeier et al. (2010), grain size fractions <100  
203  $\mu\text{m}$  filter out large aggregate grains that may be contaminants, and this study uses these grain size  
204 fractions for thermal decomposition and sequential dissolution.

205

## 206 **Characterization methods**

207

208 Alkalinity screening, cathodoluminescence microscopy and thermal gravimetric analysis, are used  
209 to characterize the mortar samples. The characterization methods are presented below.

210

### 211 Alkalinity screening

212

213 Alkalinity is an indicator for late-in-formation pyrogenic carbonates (Labeyrie and Delibrias 1964;  
214 Ringbom et al. 2011; Lichtenberger et al. 2015). Roughly 10 ml of deionized water suspends  
215 roughly 200 mg of the 300–500  $\mu\text{m}$  grainsize fraction. Strips of pH indicator paper and two drops  
216 of 2 % phenolphthalein in alcohol assess the samples' alkalinity. For alkaline samples, the  
217 phenolphthalein gives a strong purple color after 5 minutes, and alkaline samples are usually  
218 rejected for AMS dating. However, this study works with some alkaline samples to study late-in-  
219 formation pyrogenic carbonates.

220

### 221 Cathodoluminescence microscopy

222

223 The 46–75  $\mu\text{m}$  grain size fraction is characterized with a stereomicroscope combined with a  
224 Cambridge Image Technology Ltd (CITL) CL8200 MK4 cold cathode cathodoluminescence (CL)  
225 device and a camera (Marshall 1988). In CL mineral grains with luminescence light up in specific  
226 colors that enable mineral identification, e.g. limestone and marble are often bright orange-red  
227 (Götze 2012; Al-Bashaireh 2013). If abundant grains of limestone or marble are identified by CL  
228 the sample may have problems with geological carbonate. Such samples are usually rejected for  
229 AMS dating, but this study works with some samples with geological carbonate. Though not done  
230 in this study, CL with a polished sample surface can study late-in-formation pyrogenic carbonates  
231 (Marshall 1988; Götze 2012).

232

233 Thermal gravimetric analysis

234

235 Before thermal decomposition, samples are characterized with thermal gravimetric analysis (TGA)  
236 (Bakolas et al. 1998; Toffolo et al. 2017; Ponce-Anton et al. 2018). The analysis takes around 10  
237 mg of the grain size fraction 46–75  $\mu\text{m}$ , and places it in a furnace equipped with a precision scale  
238 and nitrogen atmosphere. At increased temperatures, an increasing fraction of the solid sample  
239 thermally decomposes to gaseous products. TGA measures loss of sample weight as function of  
240 temperature. This study uses the TGA instrument, Tainstruments SDT Q600, at the department of  
241 Inorganic Chemistry at Åbo Akademi University. Notice that the TGA instrument cannot collect  
242  $\text{CO}_2$  for radiocarbon dating, so the TGA is made on a small aliquot of the grain size fraction, and  
243 the actual thermal decomposition for radiocarbon dating on a larger aliquot. The result from the  
244 TGA method establishes the temperature interval where a mortar sample's carbonates thermally  
245 decompose and release  $\text{CO}_2$ . This is important information when operating the temperature and  $\text{CO}_2$

246 collection of the thermal decomposition preparation method (explained below). The result section  
247 on TGA elaborates further on different stages of mass loss during thermal decomposition of mortar  
248 samples.

249

## 250 **Preparation methods**

251

### 252 Sequential dissolution (SQ)

253

254 This project uses the well-tried sequential dissolution (SQ) method as comparison to thermal  
255 decomposition. In short, the method works by a single injection of excessive 85% phosphoric acid  
256 on a powder prepared from the sample (Ringbom et al. 2014; Lindroos et al. 2018). The pre-  
257 treatment section describes production of powders, and we use several grain size windows below  
258 100  $\mu\text{m}$  and lime lumps, see Table 1. Late-in-formation pyrogenic carbonate, binder carbonate and  
259 geological carbonate dissolve with different reaction rates, and contribute differently to different  
260  $\text{CO}_2$  fractions collected throughout the dissolution. For example geological carbonate dissolves  
261 more slowly, and its contribution increases in the later fractions of SQ. Ringbom et al. (2014)  
262 describe the SQ method in more detail.

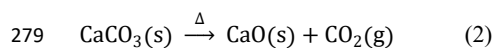
263

### 264 Thermal decomposition (TD)

265

266 Figure 1 illustrates the experimental setup for sample preparation with thermal decomposition (TD).  
267 The system is similar to systems used for SQ, with the laboratory furnace replacing the dissolution  
268 reactor flask (Heinemeier et al. 2010; Ringbom et al. 2014). TD places the selected grain size  
269 fraction in a quartz tube and fixates it with a lump of quartz wool. A hose connects the quartz tube  
270 and the vacuum system. When the system's vacuum is sufficient, the furnace slowly increases the  
271 temperature of the sample. When the preparation's start-temperature is reached, the pressure gauge  
272 monitors the release of gaseous products from TD. Characterization by TGA establishes sample-  
273 specific start-temperatures, usually around 550-650 °C, where the mortar's carbonates start  
274 releasing CO<sub>2</sub>. Other studies report TD of anthropogenic carbonate starting in the range 500-550 °C  
275 (Toffolo et al. 2017; Ricci et al. 2020). Chemistry literature describes the release of CO<sub>2</sub> by TD of  
276 calcium carbonate with equation 2, and that it happens at temperatures in range 680-875 °C  
277 (Murthy et al. 1994; Rao 1996; Karunadasa et al. 2019):

278



280

281 FigureThermalSetup

282

283 When the amount of CO<sub>2</sub> is sufficient for AMS dating (in range 0.1 mgC - 1.0 mgC), liquid  
284 nitrogen freezes out a fraction and a blowtorch seals the fraction in a glass vial. The furnace is  
285 thermostat regulated, and it holds a set temperature. As long as the sample continues to release CO<sub>2</sub>  
286 the temperature is kept constant, and only when CO<sub>2</sub> release stops the temperature is carefully  
287 increased to resume TD. In this way, the early fractions contain CO<sub>2</sub> from sample phases that

288 thermally decompose at lower temperatures, while later fractions contain CO<sub>2</sub> from sample phases  
289 that thermally decompose at higher temperatures. This aligns with Toffolo et al. (2020) and Ricci et  
290 al. (2020) discussing TD of different mortar phases in different temperature ranges, for example  
291 organic phase up to 500 °C, LDH phase around 500-550 °C, pyrogenic carbonates (e.g. lime mortar  
292 binder) in the range 500-650 °C and marble in range 700-800 °C. In our TD preparation a typical  
293 start-temperature is around 550-650 °C, the temperature increments are around 10-20 °C, it takes 5-  
294 15 min to produce a fraction, and a sample is exhausted somewhere between 800-900 °C. As a  
295 variation sample Merida003 has start-temperature at room temperature, see the results section.

296 Calcite backgrounds are also thermally decomposed. The backgrounds are compiled to a  
297 background correction used for TD radiocarbon determinations (Donahue et al. 1990; Brown and  
298 Southon 1997; Toffolo et al. 2020).

299

300 Preheating followed by sequential dissolution (P+SQ)

301

302 Ricci et al. (2020) discuss a thermal treatment at 550 °C to break down the LDH structure and  
303 release the associated carbonate anions, e.g. in a magnesium-rich mortar. Inspired hereof,  
304 preheating followed by sequential dissolution (P+SQ) is attempted for sample Merida003, which is  
305 a dolomitic mortar somewhat similar to the magnesium-rich samples discussed by Ricci et al.  
306 (2020). The sample is preheated to 620 °C and the temperature is maintained for half an hour. This  
307 temperature was chosen for sample Merida003, because it is the lowest temperature producing  
308 enough CO<sub>2</sub> from preheating for a datable fraction. The sample then cools to room temperature  
309 while still in vacuum, see Figure 1. One then breaks vacuum, quickly transfers the sample to a

310 reactor flask in the SQ setup and reapplies vacuum. SQ then prepares the preheated sample as  
311 described in the materials and methods section on sequential dissolution.

312

### 313 **Graphitization and AMS dating**

314

315 Graphitization reactors convert the produced CO<sub>2</sub> fractions to graphite using hydrogen and an iron  
316 catalyst (Vogel et al. 1984). A pneumatic press presses the graphite into AMS-cathodes, and they  
317 are radiocarbon dated at Aarhus AMS Centre using the centre's HVE 1MV accelerator (Olsen et al.  
318 2017), except for samples TTK004, TTK004Li and Kimito004Li by SQ that were dated in Zürich  
319 using the MICADAS machine at the Laboratory of Ion Beam Physics (Synal et al. 2007). For each  
320 sample multiple fractions are dated, so one can evaluate conclusiveness as described in the  
321 discussion. The online program OxCal 4.4 with the IntCal20 calibration curve calculates calendar  
322 date from radiocarbon determinations (Bronk Ramsey 2009; Reimer et al. 2020).

323

## 324 **RESULTS**

325

326 This section presents results from characterization and radiocarbon dating of the selected samples.  
327 Radiocarbon profiles illustrate the dated CO<sub>2</sub> fractions, and the incremental heating method in  
328 potassium-argon dating inspires the style of plotting in Figures 5-7 (Foland 1983). Each box  
329 illustrates a radiocarbon-dated CO<sub>2</sub> fraction. The horizontal extent of a fraction illustrates the  
330 cumulative CO<sub>2</sub> fraction released prior to the fraction and after the fraction. The vertical extend of a



331 fraction illustrates the 68 % confidence interval of the determined  $F^{14}C$  ( $^{14}C$  age =  $-8033 \cdot \ln F^{14}C$ ),  
332 Text annotates the temperature reached during production of the corresponding TD fraction.

333

### 334 **Characterization**

335

336 Figure 2 shows CL images screening for limestone or marble aggregate that may carry geological  
337 carbonate contamination. Figure 2B shows the CL image for sample J13-ESM-1. Unfortunately,  
338 some types of limestone at Jerash do not have the typical red-orange luminescence (Al-Bashaireh  
339 and Hodgins 2012; Lichtenberger et al. 2015). Therefore, CL cannot rule out geological carbonate  
340 for sample J13-ESM-1. Alkalinity screens samples for late-in-formation pyrogenic carbonates, and  
341 Table 2 summarizes the characterization results for CL and alkalinity. There are potential problems  
342 with most samples, and usually one would reject these for AMS dating. However, the aim is to  
343 investigate TD for recurring challenges in mortar dating.

344

345 FigureCathodoluminescence

346

347 TableCharacterization

348

349 Figure 3 shows the results from TGA, where samples loose mass through TD. The samples show  
350 drying of pore space water and water of crystallization for temperature below 200 °C (Bakolas et al.  
351 1998; Paama et al. 1998). From 200-600 °C, the TGA curves decrease further because of

352 decomposition of OH<sup>-</sup> groups, which may come from unhardened slaked lime or hydraulic mortar  
353 minerals, e.g. calcium silicate hydrate (Dodson 1990; Massazza 2003; Ponce-Anton et al. 2018).  
354 Near 640-650 °C the TGA curves start a dramatic loss of weight, and much of this is attributed to  
355 TD of CaCO<sub>3</sub> (Bakolas et al. 1998; Paama et al. 1998; Ponce-Anton et al. 2018). It is interesting  
356 that this loss of mass starts below the temperature interval (680-875 °C) reported for TD of CaCO<sub>3</sub>  
357 in chemistry literature, and the discussion elaborates further on this. Just below 800 °C, the  
358 samples' carbonate is exhausted and decomposition ceases. The TGA curves helps decide the start-  
359 temperatures reported in the below sections on TD of selected samples.

360

361 FigureTGA

362

### 363 **Thermal decomposition backgrounds**

364

365 TD has its own background correction compiled from calcite backgrounds of various sample sizes.  
366 In Figure 4, the measured F<sup>14</sup>C values are plotted as a function of inverse sample mass, and the  
367 fitted function is used to correct TD radiocarbon determinations (Donahue et al. 1990; Brown and  
368 Southon 1997; Toffolo et al. 2020).

369

370 FigureBackground

371

### 372 **Thermal decomposition and geological carbonate**

373

374 Figure 5A shows radiocarbon profiles with TD and SQ for sample TTK006 from Turku Cathedral,  
375 Finland. There is also a radiocarbon profile with SQ for sample TTK005, and the two samples are  
376 from the same wall. Interpolation of the IntCal20 curve calculates expected  $F^{14}C$  for Turku  
377 Cathedral (Reimer et al. 2020), and this yields  $F^{14}C=0.9212\pm0.0013$  for the inauguration in 1300  
378 AD and  $F^{14}C=0.9254\pm0.0012$  for the destruction in 1318 AD.

379 The SQ profiles for TTK005 and TTK006 show decreasing  $F^{14}C$  for later fractions, while the 1<sup>st</sup>  
380 and 2<sup>nd</sup> fractions are closer to the expected  $F^{14}C$ . The geological carbonate identified by CL is a  
381 probable explanation for late fractions with lower  $F^{14}C$ , see Table 2. The first minimum (3<sup>rd</sup> CO<sub>2</sub>  
382 fraction) in the SQ profile for sample TTK005 has been interpreted as aggregate marble  
383 contamination, and the minimum defined by the last (5<sup>th</sup>) fraction as calcination residues from  
384 incomplete lime burning (Lindroos et al. 2018).

385 Figure 5A also shows TD for sample TTK006. The furnace heats sample TTK006 to 650 °C, as  
386 suggested by TGA in Figure 3, and collection of fractions starts. The first temperature interval, from  
387 650-680 °C, produces too little CO<sub>2</sub> for AMS dating. The TD radiocarbon profile for TTK006 is  
388 also decreasing for later fractions, and it shows multiple minima and maxima as do the SQ profile  
389 of sample TTK005. All TD CO<sub>2</sub> fractions seem affected by geological carbonate because they have  
390 lower  $F^{14}C$  than expected.

391

392 FigureDeadCarbon

393

394 Figure 5B shows TD and SQ of sample J13-ESM-1, a mortar-cover cast around a water pipe in  
395 Jerash in Jordan (Lichtenberger et al. 2015). The sample's expected  $F^{14}C=0.8070\pm0.0025$  comes  
396 from a charcoal sample embedded in the mortar (Lichtenberger et al. 2015). According to Al  
397 Bashairh (2013) charcoal in mortar can be used for dating, if short-lived bushes were burned and  
398 not old wood. The first fraction of SQ and charcoal are similar in  $F^{14}C$ , while later fractions in the  
399 SQ profile has lower  $F^{14}C$  values. This behavior matches a sample influenced by geological  
400 carbonate. As explained in the characterization results section CL cannot rule out geological  
401 carbonate for this sample, because some types of limestone at Jerash are without a luminescence  
402 property. Yaseen et al. (2013) and Lichtenberger et al. (2015) find limestone sand and gravel  
403 aggregate in most Jerash mortars, and this could be the case for sample J13-ESM-1. The sample  
404 was not found alkaline, so it is unlikely that late-in-formation pyrogenic carbonates are abundant,  
405 see Table 2.

406 For TD, the furnace heats sample J13-ESM-1 to 600 °C, lower than suggested by TGA in Figure 3,  
407 and collection of fractions starts. The TD radiocarbon profile is also decreasing in  $F^{14}C$  for later  
408 fractions, and geological carbonate is a possible explanation. Interestingly, the first fraction of TD  
409 has a higher  $F^{14}C$  than expected, while the first fraction of SQ has not.

#### 411 **Thermal decomposition and late-in-formation pyrogenic carbonates**

412  
413 Figure 6A shows TD and SQ of sample Kastel09 from Kastelholm castle in Finland. Figure 6A also  
414 shows a SQ profile for sample Kastel10, and the two samples originate from the same structural  
415 unit. Interpolation of the IntCal20 curve calculates the expected  $F^{14}C=0.9253\pm0.0012$  from the first  
416 written source on Kastelholm in 1388 AD (Hausen 1910). Allowing 10 years for construction, or a

417 delay from construction to first written source, the year 1378 AD has expected  
418  $F^{14}C=0.9217\pm 0.0011$ . Lindroos et al. (2020a) report alkalinity, fire damage and limited limestone  
419 contamination for Kastelholm mortar. ~~Lindroos et al. (2020a) found young carbonates from fire~~  
420 ~~damage and reactivation in mortar from Kastelholm castle.~~ CL finds few red grains in both samples,  
421 Kastel10 is alkaline, and Kastel09 is not alkaline, see Table 2. In Figure 6A, the two SQ profiles  
422 have fractions with higher  $F^{14}C$  values than expected, and late-in-formation pyrogenic carbonate  
423 from alkalinity or fire damage is a likely explanation. Notice that higher than expected  $F^{14}C$  mostly  
424 affects sample Kastel10, which is alkaline.

425 In TD, the furnace heats sample Kastel09 to 550 °C, lower than suggested by TGA in Figure 3, and  
426 collection of CO<sub>2</sub> fractions starts. The first temperature interval from 550-680 °C, yields too little  
427 CO<sub>2</sub> for AMS dating. Comparing with SQ profiles, the TD profile is quite flat and no fractions have  
428 higher  $F^{14}C$  than expected.

429

430 FigureYoungCarbonates

431

432 Figure 6C shows TD and SQ of the lime lump sample Kimito004Li from Kimito church in Finland.  
433 Interpolation of the IntCal20 curve calculates the expected  $F^{14}C=0.9317\pm 0.0012$  from the year 1400  
434 AD, which is the beginning of the 1<sup>st</sup> half of the 15<sup>th</sup> century. Likewise, the year 1450 AD, which is  
435 the end of the 1<sup>st</sup> half of the 15<sup>th</sup> century, has expected  $F^{14}C=0.9480\pm 0.0012$ . In Figure 6C, the SQ  
436 profile is in range of the expected  $F^{14}C$ , but later fractions show decreasing  $F^{14}C$  values. CL rules  
437 out geological carbonates, so a possible explanation is late-in-formation pyrogenic carbonate  
438 shifting early fractions to higher  $F^{14}C$ . Alkalinity screening to support this is unavailable, as the  
439 lime lump was exhausted.

440 For TD, the furnace heats sample Kimito004Li to 600 °C, lower than suggested by TGA in Figure  
441 3, and collection of fractions starts. The TD profile is in range of the expected  $F^{14}C$ , and more  
442 homogenous than the SQ profile.

443

#### 444 **Preheating followed by sequential dissolution**

445

446 In relation to preheating, we test if it is possible to produce  $CO_2$  below the start temperature  
447 suggested by TGA. Thus TD preparation of sample Merida003 starts  $CO_2$  collection from room  
448 temperature to 620 °C.

449 Figure 7A shows sample Merida003 with TD and SQ. Interpolation on the IntCal20 curve  
450 calculates the expected  $F^{14}C=0.7841\pm0.0014$  for the year 69 AD, which is the beginning of the  
451 Flavian dynasty, and the expected  $F^{14}C=0.7859\pm0.0014$  for the year 96 AD, which is the end of the  
452 Flavian dynasty. Early fractions in the SQ profile have higher  $F^{14}C$  than expected. Characterization  
453 found this sample alkaline, so late-in-formation pyrogenic carbonates are a likely explanation. The  
454 TD profile starts  $CO_2$  collection from room temperature to 620 °C, and all fractions have higher  
455  $F^{14}C$  values than expected, especially the three earliest fractions. Again late-in-formation pyrogenic  
456 carbonates are a likely explanation.

457 Figure 7B shows sample Merida003 with SQ (repeated) and P+SQ (preheated to 620°C). A  
458 considerable part of the P+SQ profile in Figure 7B is close to the expected  $F^{14}C$ . The  $CO_2$  thermally  
459 decomposed during preheating was collected and radiocarbon dated to  $F^{14}C=0.8437\pm0.0049$ , see  
460 Table 1 for sample run no. Merida003 PSQ1.T1.

461

462 FigurePreheating

463

## 464 **DISCUSSION**

465

466 Table 2 summarizes characterization results, and this identifies potential problems with limestone,  
467 marble or alkalinity for most samples. To investigate TD for problematic mortar no samples are  
468 rejected for dating. As mention in the results section, CL cannot rule out geological carbonate for  
469 sample J13-ESM-1 because of non-luminescent limestone at Jerash. Apart from this, the sample  
470 characterization is very useful in identifying problems that enable evaluation of radiocarbon  
471 profiles, e.g. fractions influenced by geological carbonate or late-in-formation pyrogenic carbonate.

472 Figure 3 shows TGA curves for mortar samples, and the dominant mass losses start around 640-  
473 650°C, which is lower than the reported start temperatures for TD of calcium carbonate, e.g. 680-  
474 700 °C (Rao 1996; Karunadasa et al. 2019). This compares to Ricci et al. (2020) and Toffolo et al.  
475 (2020) discussing pyrogenic carbonates decomposing at lower temperatures than geological  
476 carbonates. As mentioned in materials and methods, Ricci et al. (2020) employ a thermal treatment  
477 at 550 °C to eliminate the carbonate fraction of LDHs, and this study experimented with preheating  
478 at 620 °C. It may be possible to do a thermal treatment closer to the start temperature of the  
479 dominant mass loss, e.g. 640-650 °C, without losing too much binder carbonate.

480 Figure 4 shows calcite backgrounds and the background correction for TD. The background  $F^{14}C$   
481 level has order of magnitude  $10^{-3}$ . Considering that ancient and medieval samples are well above  
482 one  $^{14}C$  half-life, i.e.  $F^{14}C > 0.5$ , the background level is satisfactory.

483 As seen in Table 1 the carbon yield of TD is significantly lower than SQ. At the same time, TD  
484 produces a sizeable amount of incondensable gas. TD of  $\text{CaCO}_3$  in a vacuum may not happen  
485 entirely as described by equation 2. Part of the carbonate may produce carbon monoxide, which  
486 liquid nitrogen cannot freeze. Future work can investigate the carbon yield of TD with oxidizing  
487 agents such as pellets of CuO or an  $\text{O}_2$  atmosphere. These may oxidize carbon monoxide to  $\text{CO}_2$   
488 and increase the yield. However, it is unknown if the addition of an oxidizing agent has an effect on  
489 TD temperatures or TD rates for late-in-formation pyrogenic carbonate, binder carbonate or  
490 geological carbonate.

491

#### 492 **Conclusiveness and accuracy**

493

494 To evaluate conclusive sample ages from the radiocarbon profiles in Figure 5-7, we use criterion I  
495 defined by Heinemeier et al. (2010):

496

497 Criterion I: The  $\text{F}^{14}\text{C}$  of the first two  $\text{CO}_2$  fractions are the same.

498

499 The conclusive radiocarbon determination for the mortar sample is then the weighted average of the  
500 first two fractions. The criterion is based on the assumption that the preparation method's chemistry  
501 have different reaction rates for late-in-formation pyrogenic carbonate, binder carbonate and  
502 geological carbonate. Here they are listed in order of decreasing reaction rate. Two  $\text{F}^{14}\text{C}$   
503 determinations are considered the same, if a chi-square test for goodness of fit evaluates that the  
504 two values are well-described by their weighted average (Bennett and Franklin 1954; Bronk



505 Ramsey 2009). Accuracy is evaluated by comparing the conclusive  $F^{14}C$  and an expected  $F^{14}C$   
506 value with the same chi-square test for goodness of fit.

507 In Figure 7, the profiles by TD, SQ and P+SQ have plateaus where 3-4 fractions show similar  $F^{14}C$ .  
508 The plateaus in the profiles by SQ and P+SQ have  $F^{14}C$  values close to the expected, see Figure 7B.  
509 It may, or it may not, be possible to formulate and use conclusiveness criteria based on plateaus.  
510 Perhaps, plateau criteria could be based on a chi-square test of fractions'  $F^{14}C$  values, or the  
511 plateau's cumulative  $CO_2$  fraction, or agreement between multiple plateaus by different preparation  
512 methods. We advise caution if one rules late plateaus conclusive because they can be inaccurate, see  
513 Merida003 (TD) in figure 7A. We did not succeed in formulating simple and objective criteria that  
514 simultaneously rule the accurate plateau in profile Merida003 (SQ) conclusive, and the inaccurate  
515 plateau in profile Merida003 (TD) inconclusive. This study therefore avoids interpretation of late  
516 plateaus.

517

### 518 **Thermal decomposition and geological carbonate**

519

520 In figure 5A, the 1<sup>st</sup> and 2<sup>nd</sup> fractions of profile TTK005 (SQ) pass conclusiveness criterion I, see  
521 Table 3, and give conclusive  $F^{14}C=0.9277\pm0.0029$ . Furthermore, this conclusive  $F^{14}C$  and the  
522 expected  $F^{14}C$  for the destruction in 1318 AD pass a chi-square test, see Table 3, so this conclusive  
523 radiocarbon determination is accurate for Turku cathedral's destruction. All profiles besides  
524 TTK005 (SQ) in Figure 5A and Figure 5B fail conclusiveness criterion I, and their results are  
525 inconclusive, see Table 3. No TD profiles for a sample with abundant geological carbonates achieve  
526 a conclusive mortar dating result. Considering these results, one can argue that TD is worse than SQ  
527 at distinguishing geological carbonate and binder carbonate.

528

529 TableConclusivenessAccuracy

530

531 **Thermal decomposition and late-in-formation pyrogenic carbonates**

532

533 In Figure 6A, the 1<sup>st</sup> and 2<sup>nd</sup> fractions of Kastel09's TD profile pass conclusiveness criterion I, and  
534 give conclusive  $F^{14}C=0.9203\pm0.0020$ , see Table 3. The conclusive  $F^{14}C$  and expected  $F^{14}C$  for 1378  
535 AD pass a chi-square test, see Table 3, so the conclusive  $F^{14}C$  is an accurate radiocarbon  
536 determination for Kastelholm castle. Figure 6B shows calibrated date of Kastel09's conclusive  
537  $F^{14}C$ , which agrees with Kastelholm castle first mentioned in written sources in 1388 AD (Hausen  
538 1910). The SQ profiles for Kastel09 and Kastel10 fail conclusiveness criterion I, and their results  
539 are inconclusive, see Table 3.

540 In Figure 6C, the profile Kimito004Li (TD) passes conclusiveness criterion I, see Table 3, and  
541 yields conclusive  $F^{14}C=0.9310\pm0.0019$ . The conclusive  $F^{14}C$  and expected  $F^{14}C$  for 1400 AD pass a  
542 chi-square test, see Table 3. Thus, the conclusive  $F^{14}C$  is an accurate radiocarbon determination for  
543 the sacristy of Kimito church. Figure 6D shows calibrated date for Kimito004Li's conclusive  $F^{14}C$ ,  
544 which has some probability in the 1<sup>st</sup> half of the 15<sup>th</sup> century AD. This agrees with the expected age  
545 of Kimito church's sacristy (Nikula 1975). The expected age is based on historical context, see the  
546 samples subsection in materials and methods section, so this is actually the first dating of Kimito  
547 church.

548 TD of mortar samples with late-in-formation pyrogenic carbonates, and limited geological  
549 carbonate, seems to improve radiocarbon profiles in Figure 6A and Figure 6C. The causes of these

550 preliminary findings have not yet been studied. Figure 7A shows TD of Merida003, where CO<sub>2</sub>  
551 collection starts at room temperature. The first three TD fractions have the highest F<sup>14</sup>C compared  
552 to the expected F<sup>14</sup>C, and likely they are affected by late-in-formation pyrogenic carbonates  
553 outgassing somewhere from room temperature to 710 °C. Secondary sodium carbonates formed in  
554 wet conditions, e.g. trona and thermonatrite (Na<sub>3</sub>H(CO<sub>3</sub>)<sub>2</sub>·2H<sub>2</sub>O and Na<sub>2</sub>(CO<sub>3</sub>)·H<sub>2</sub>O, respectively)  
555 and vaterite (CaCO<sub>3</sub>) after fire damage, have lower decomposing temperatures (Maciejewski et al.  
556 1994; Hartman et al. 2001; Lindroos et al. 2012). This can explain how Figure 6A and Figure 6C  
557 improve, as these experiments start CO<sub>2</sub> collection around 600 °C. Below this temperature some  
558 late-in-formation pyrogenic carbonates may drive off, and not affect fractions collected later.

559

#### 560 **Preheating followed by sequential dissolution**

561

562 In Figure 7 none of the Merida003 profiles by TD, SQ or P+SQ pass conclusiveness criterion I, and  
563 their radiocarbon determinations are inconclusive, see Table 3. Many fractions have higher F<sup>14</sup>C  
564 than expected, and it is surprising that the entire TD profile for Merida003 has higher F<sup>14</sup>C than  
565 expected. The Merida samples are very hard, and Lindroos et al. (2020b) discuss poor permeability  
566 for CO<sub>2</sub> and delayed hardening, which could be an explanation for higher F<sup>14</sup>C than expected. For  
567 dolomitic mortars LDHs can contain carbonate from exchanged atmospheric CO<sub>2</sub> (Artioli et al.  
568 2017; Ponce-Anton et al. 2018). Ricci et al. (2020) and Toffolo et al. (2020) find that carbonate  
569 captured by LDHs decomposes around 500-550 °C, so one would expect this to contribute to the  
570 first TD fraction only.

571 Figure 7B presents results from P+SQ preparation of sample Merida003. P+SQ improves the  
572 profile, which shows less late-in-formation pyrogenic carbonate than SQ. It seems that some late-in-

573 formation pyrogenic carbonate decomposed in the preheating, but the P+SQ profile still fails  
574 conclusiveness criterion I. It would be interesting to investigate preheating at a temperature above  
575 620 °C.

576

## 577 **CONCLUSION**

578

579 TD in vacuum can extract CO<sub>2</sub> from a mortar sample, and TGA curves are useful for choosing the  
580 experimental parameters. TD in vacuum has a significantly lower carbon yield than SQ, and this  
581 study used larger sample aliquots for TD than SQ.

582 TD is not successful in preparing samples with geological carbonate. As seen in Figure 5A and  
583 Figure 5B binder carbonate and geological carbonate does not behave sufficiently different in  
584 preparation by TD.

585 This study finds an interesting interaction between TD and late-in-formation pyrogenic carbonates  
586 from alkalinity or fire damage. Figure 7A shows TD driving off material with higher F<sup>14</sup>C than the  
587 rest of the sample at temperatures from room temperature to 710 °C. In this way, Kastel09 and  
588 Kimito004Li may have had their late-in-formation pyrogenic carbonates removed below the  
589 preparation's start temperature, and the two samples are conclusively dated in Figure 6A and Figure  
590 6C. The conclusive radiocarbon determinations for Kastelholm castle and Kimito church accurately  
591 agree with the buildings' expected ages.

592 Another application is P+SQ, which preheats to remove late-in-formation pyrogenic carbonates  
593 prior to sequential dissolution. In Figure 7B, the preheating (at 620 °C for half an hour) removes

594 some late-in-formation pyrogenic carbonates, but not enough for the P+SQ profile to pass  
595 conclusiveness criterion I.

596

## 597 **ACKNOWLEDGEMENTS**

598

599 This work was supported by the Danish National Research Foundation under the grant D NRF119 -  
600 Centre of Excellence for Urban Network Evolutions (UrbNet).

601 This study is extremely grateful to Rubina Raja, Aarhus University, and Achim Lichtenberger,  
602 Ruhr-Universität Bochum. Their work and directorship at the Danish–German Jerash Northwest  
603 Quarter project made Jerash mortar samples available to this study.

604 Åsa Ringbom directed the sampling in Kimito and Kastelholm within the project "International  
605 Mortar Dating" and Stig Dreijer sponsored the project. Pia Sjöberg and Bo Ossian Lindberg guided  
606 the sampling in Kimito.

607

## 608 **REFERENCES**

- 609 Al-Bashaireh K, Hodgins GW. 2012. LIME MORTAR AND PLASTER: A RADIOCARBON DATING TOOL FOR  
610 DATING NABATEAN STRUCTURES IN PETRA, JORDAN. *Radiocarbon* 54(3-4):905-14.
- 611 Al-Bashaireh K. 2013. PLASTER AND MORTAR RADIOCARBON DATING OF NABATEAN AND ISLAMIC  
612 STRUCTURES, SOUTH JORDAN. *Archaeometry* 55(2):329-54.
- 613 Artioli G, Secco M, Addis A, Bellotto M. 2017. Role of hydrotalcite-type layered double hydroxides in  
614 delayed pozzolanic reactions and their bearing on mortar dating. In: Gruyter Wd, editor.  
615 *Cementitious Materials: Composition, Properties, Application*. Berlin, Germany.
- 616 Bakolas A, Biscontin G, Moropoulou A, Zendri E. 1998. Characterization of structural byzantine mortars by  
617 thermogravimetric analysis. *Thermochimica Acta* 321(1-2):151-60.
- 618 Baxter MS, Walton A. 1970. RADIOCARBON DATING OF MORTARS. *Nature* 225(5236):937-8.
- 619 Bennett CA, Franklin NL. 1954. *Statistical analysis in chemistry and the chemical industry*. New York: Wiley.
- 620 Bronk Ramsey C. 2009. Bayesian Analysis of Radiocarbon Dates. *Radiocarbon* 51(1):337-60.

Formatted: Danish

621 Brown TA, Southon JR. 1997. Corrections for contamination background in AMS 14C measurements.  
622 Nuclear Instruments and Methods in Physics Research Section B: Beam Interactions with Materials  
623 and Atoms 123(1):208 - 13.

624 Capello R-MD, Galán MB. El anfiteatro de Augusta Emerita: rasgos arquitectónicos y problemática  
625 urbanística y cronológica, en el anfiteatro en la Hispania romana; 1995; Mérida, 26-28 de  
626 Noviembre de 1992. p 247-64.

627 Dodson VH. 1990. Concrete admixtures: Springer US.

628 Donahue DJ, Linick TW, Jull AJT. 1990. Isotope-Ratio and Background Corrections for Accelerator Mass  
629 Spectrometry Radiocarbon Measurements. Radiocarbon 32:135-42.

630 Foland KA. 1983. AR-40/AR-39 INCREMENTAL HEATING PLATEAUS FOR BIOTITES WITH EXCESS ARGON.  
631 Isotope Geoscience 1(1):3-21.

632 Folk RL, Valastro S. 1976. Successful Technique for Dating of Lime Mortar by Carbon-14. Journal of Field  
633 Archaeology 3(2):195-201.

634 Gardberg CJ, Simo H, Welin PO. 2000. Nationalhelgedomen. Åbo domkyrka 1300-2000. Helsingfors.

635 Götze J. 2012. Application of Cathodoluminescence Microscopy and Spectroscopy in Geosciences.  
636 Microscopy and Microanalysis 18(6):1270-84.

637 Hajdas I, Lindroos A, Heinemeier J, Ringbom Å, Marzaioli F, Terrasi F, Passariello I, Capano M, Artioli G,  
638 Addis A, Secco M, Michalska D, Czernik J, Goslar T, Hayen R, Van Strydonck M, Fontaine L, Boudin  
639 M, Maspero F, Panzeri L, Galli A, Urbanova P, Guibert P. 2017. PREPARATION AND DATING OF  
640 MORTAR SAMPLES-MORTAR DATING INTER-COMPARISON STUDY (MODIS). Radiocarbon  
641 59(6):1845-58.

642 Hale J, Heinemeier J, Lancaster L, Lindroos A, Ringbom Å. 2003. Dating ancient mortar. American Scientist  
643 91(3):130-7.

644 Hartman M, Trnka O, Veselý V, Svoboda K. 2001. THERMAL DEHYDRATION OF THE SODIUM CARBONATE  
645 HYDRATES. Chemical Engineering Communications 185(1):1-16.

646 Hausen RT. 1890. Registrum ecclesiae Aboensis - Åbo domkyrkas svartbok. Helsingfors.

647 Hausen RT. 1910. Finlands medeltidsurkunder: Finlands Statsarkiv.

648 Heinemeier J, Jungner H, Lindroos A, Ringbom Å, von Konow T, Rud N. 1997. AMS C-14 dating of lime  
649 mortar. Nuclear Instruments & Methods in Physics Research Section B-Beam Interactions with  
650 Materials and Atoms 123(1-4):487-95.

651 Heinemeier J, Ringbom Å, Lindroos A, Sveinbjornsdottir AE. 2010. SUCCESSFUL AMS C-14 DATING OF NON-  
652 HYDRAULIC LIME MORTARS FROM THE MEDIEVAL CHURCHES OF THE ALAND ISLANDS, FINLAND.  
653 Radiocarbon 52(1):171-204.

654 Jones BW, Milns RD, Suetonius. 2002. The Flavian Emperors: Bristol Classical Press.

655 Karunadasa KSP, Manoratne CH, Pitawala H, Rajapakse RMG. 2019. Thermal decomposition of calcium  
656 carbonate (calcite polymorph) as examined by in-situ high-temperature X-ray powder diffraction.  
657 Journal of Physics and Chemistry of Solids 134:21-8.

658 Labeyrie J, Delibrias G. 1964. DATING OF OLD MORTARS BY CARBON-14 METHOD. Nature 201(492):742.

659 Lichtenberger A, Lindroos A, Raja R, Heinemeier J. 2015. Radiocarbon analysis of mortar from Roman and  
660 Byzantine water management installations in the Northwest Quarter of Jerash, Jordan. Journal of  
661 Archaeological Science-Reports 2:114-27.

662 Lindroos A, Ringbom Å, Kaisti R, Heinemeier J, Hodgins G, Brock F. 2011. Archaeology and History of  
663 Churches in Baltic Region. Symposium, June 8-12, 2010, Visby, Sweden. In: HANSSON J, RANTA H,  
664 editors. ARCHAEOLOGY AND HISTORY OF CHURCHES IN BALTIC REGION. SYMPOSIUM, JUNE 8-12,  
665 2010, VISBY, SWEDEN. Visby: iVisby Tryckeri AB. p 108-21.

666 Lindroos A, Regev L, Oinonen M, Ringbom Å, Heinemeier J. 2012. C-14 DATING OF FIRE-DAMAGED  
667 MORTARS FROM MEDIEVAL FINLAND. Radiocarbon 54(3-4):915-31.

668 Lindroos A, Ringbom Å, Heinemeier J, Hodgins G, Sonck-Koota P, Sjöberg P, Lancaster L, Kaisti R, Brock F,  
669 Ranta H, Caroselli M, Lugli S. 2018. RADIOCARBON DATING HISTORICAL MORTARS: LIME LUMPS  
670 AND/OR BINDER CARBONATE? Radiocarbon 60(3):875-99.

Formatted: Danish

Formatted: Danish

671 Lindroos A, Ringbom Å, Heinemeier J, Hajdas I, Olsen J. 2020a. DELAYED HARDENING AND REACTIVATION  
672 OF BINDER CALCITE, COMMON PROBLEMS IN RADIOCARBON DATING OF LIME MORTARS.  
673 Radiocarbon:1-13.

674 Lindroos A, Heinemeier J, Ringbom Å, Daugbjerg TS, Hajdas I. 2020b. The Roman amphitheatre in Mérida,  
675 Spain - Augustan or Flavian? Radiocarbon Dating Results on Mortar Carbonate. To be printed in  
676 Geochronometria.

677 Maciejewski M, Oswald H-R, Reller A. 1994. Thermal transformations of vaterite and calcite.  
678 Thermochemica Acta 234:315-28.

679 Marshall DJ. 1988. Cathodoluminescence of Geological Materials. Geological Magazine 128:404-5.

680 Marzaioli F, Lubritto C, Nonni S, Passariello I, Capano M, Terrasi F. 2011. Mortar Radiocarbon Dating:  
681 Preliminary Accuracy Evaluation of a Novel Methodology. Analytical Chemistry 83(6):2038-45.

682 Massazza F. 2003. Pozzolana and Pozzolanic Cements. In: Hewlett PC, editor. Lea's chemistry of cement and  
683 concrete: Butterworth-Heinemann. p 471-635.

684 Mateos CP. 2001. Augusta Emerita. La investigación arqueológica en un ciudad de época romana. Archivo  
685 Espanol de Arqueología 74:183-208.

686 Michalska D, Czernik J, Goslar T. 2017. METHODOLOGICAL ASPECT OF MORTARS DATING (POZNAN,  
687 POLAND, MODIS). Radiocarbon 59(6):1891-906.

688 Murthy MS, Marish BR, Rajanandam KS, Kumar K. 1994. INVESTIGATION ON THE KINETICS OF THERMAL-  
689 DECOMPOSITION OF CALCIUM-CARBONATE. Chemical Engineering Science 49(13):2198-204.

690 Nikula S. 1973. Finlands kyrkor 7. Borgå stift del I. Åbolands prosteri I.: Museiverket.

691 Nikula S. 1975. Finlands kyrkor 8. Borgå stift del II. Åbolands prosteri II.: Museiverket.

692 Olsen J, Tikhomirov D, Grosen C, Heinemeier J, Klein M. 2017. Radiocarbon Analysis on the New AARAMS  
693 1MV Tandetron. Radiocarbon 59(3):905-13.

694 Ortega LA, Zuluaga MC, Alonso-Olazabal A, Murelaga X, Insausti M, Ibanez-Etxeberria A. 2012. HISTORIC  
695 LIME-MORTAR C-14 DATING OF SANTA MARIA LA REAL (ZARAUTZ, NORTHERN SPAIN): EXTRACTION  
696 OF SUITABLE GRAIN SIZE FOR RELIABLE C-14 DATING. Radiocarbon 54(1):23-36.

697 Ponce-Anton G, Ortega LA, Zuluaga MC, Alonso-Olazabal A, Solaun JL. 2018. Hydrotalcite and  
698 Hydrocalumite in Mortar Binders from the Medieval Castle of Portilla (Alava, North Spain): Accurate  
699 Mineralogical Control to Achieve More Reliable Chronological Ages. Minerals 8(8).

700 Paama L, Pitkänen I, Rönkkömäki H, Perämäki P. 1998. Thermal and infrared spectroscopic characterization  
701 of historical mortars. Thermochemica Acta 320(1-2):127-33.

702 Rao TR. 1996. Kinetics of calcium carbonate decomposition. Chemical Engineering & Technology 19(4):373-  
703 7.

704 Reimer PJ, Austin WEN, Bard E, Bayliss A, Blackwell PG, Bronk Ramsey C, Butzin M, Cheng H, Edwards RL,  
705 Friedrich M, Grootes PM, Guilderson TP, Hajdas I, Heaton TJ, Hogg AG, Hughen KA, Kromer B,  
706 Manning SW, Muscheler R, Palmer JG, Pearson C, van der Plicht J, Reimer RW, Richards DA, Scott  
707 EM, Southon JR, Turney CSM, Wacker L, Adolphi F, Büntgen U, Capano M, Fahrni SM, Fogtmann-  
708 Schulz A, Friedrich R, Köhler P, Kudsk S, Miyake F, Olsen J, Reinig F, Sakamoto M, Sookdeo A,  
709 Talamo S. 2020. The IntCal20 Northern Hemisphere Radiocarbon Age Calibration Curve (0–55 cal  
710 kBP). Radiocarbon 62(4):725-57.

711 Ricci G, Secco M, Marzaioli F, Terrasi F, Passariello I, Addis A, Lampugnani P, Artioli G. 2020. The Cannero  
712 Castle (Italy): Development of Radiocarbon Dating Methodologies in the Framework of the Layered  
713 Double Hydroxide Mortars. Radiocarbon 62(3):617-31.

714 Ringbom Å, Hale J, Heinemeier J, Lindroos A, Brock F. 2006. Mortar dating in archaeological studies of  
715 Classical and Medieval structures. Second International Congress on Construction History.  
716 Cambridge. p 2613-34.

717 Ringbom Å, Heinemeier J, Lindroos A, Brock F. 2011. Mortar Dating and Roman pozzolana, Results and  
718 Interpretations. Commentationes Humanarum Litterarum 128:187-208.

719 Ringbom Å, Lindroos A, Heinemeier J, Sonck-Koota P. 2014. 19 YEARS OF MORTAR DATING: LEARNING  
720 FROM EXPERIENCE. Radiocarbon 56(2):619-35.

Formatted: Danish

721 Sonninen EPE, Jungner H. Dating of Mortar and Bricks, an Example from Finland. In: Maniatis Y, editor;  
722 1989; Amsterdam-Oxford-New York-Toronto. p 99-107.  
723 Stuiver M, Smith C. Radiocarbon dating of ancient mortar and plaster; 1965; Washington DC.  
724 Synal HA, Stocker M, Suter M. 2007. MICADAS: A new compact radiocarbon AMS system. Nuclear  
725 Instruments & Methods in Physics Research Section B-Beam Interactions with Materials and Atoms  
726 259(1):7-13.  
727 Toffolo MB, Regev L, Mintz E, Poduska KM, Shahack-Gross R, Berthold C, Miller CE, Boaretto E. 2017.  
728 Accurate Radiocarbon Dating of Archaeological Ash Using Pyrogenic Aragonite. Radiocarbon  
729 59(1):231-49.  
730 Toffolo MB, Regev L, Mintz E, Kaplan-Ashiri I, Berna F, Dubernet S, Yan X, Regev J, Boaretto E. 2020.  
731 Structural Characterization and Thermal Decomposition of Lime Binders Allow Accurate  
732 Radiocarbon Age Determinations of Aerial Lime Plaster. Radiocarbon 62(3):633-55.  
733 Van Strydonck M, Dupas M, Dauchotdehon M, Pachiaudi C, Marechal J. 1986. THE INFLUENCE OF  
734 CONTAMINATING (FOSSIL) CARBONATE AND THE VARIATIONS OF DELTA-C-13 IN MORTAR DATING.  
735 Radiocarbon 28(2A):702-10.  
736 Vogel JS, Southon JR, Nelson DE, Brown TA. 1984. PERFORMANCE OF CATALYTICALLY CONDENSED CARBON  
737 FOR USE IN ACCELERATOR MASS-SPECTROMETRY. Nuclear Instruments & Methods in Physics  
738 Research Section B-Beam Interactions with Materials and Atoms 5(2):289-93.  
739 Yaseen IAB, Al-Amoush H, Al-Farajat M, Mayyas A. 2013. Petrography and mineralogy of Roman mortars  
740 from buildings of the ancient city of Jerash, Jordan. Construction and Building Materials 38:465 -  
741 71.

742

743

#### 744 CAPTIONS

745 Table 1: Samples, aliquots and radiocarbon dates. It was not possible to look up the sequential  
746 dissolution mass of the samples dated before 2008. Mortar samples with TD in the sample run no.  
747 column were prepared with TD, and similarly for SQ and P+SQ. SQ radiocarbon dates taken from  
748 Lindroos et al. (2011; 2012; 2020b; 2020a), Ringbom et al. (2006) and Lichtenberger et al. (2015).

749

750 Figure 1: The experimental setup for sample preparation by thermal decomposition. Figure inspired  
751 by Ringbom et al. (2014).

752

Formatted: Danish

Formatted: Danish

Field Code Changed

Formatted: Danish

Field Code Changed



753 Figure 2: CL images for the samples TTK006, J13-ESM-1, Kastel09, Kastel10, Kimito004Li and  
754 Merida003. **A** TTK006, 46-75  $\mu\text{m}$ . Brown-grey binder calcite and orange marble calcite. The blue  
755 grain is quartz. **B** J13-ESM-1, 46-75  $\mu\text{m}$ . The sample has no luminescence. **C-D** Kastel09 and  
756 Kastel10, respectively, 46-75  $\mu\text{m}$ . Brown grains are binder calcite and red ones limestone. Blue is  
757 quartz and green is feldspar. **E** Kimito004Li, crushed lime lump. Dark red is binder calcite. **F**  
758 Merida003, 46-75  $\mu\text{m}$ , with marble splinter yellow and dolomite red. Blue, quartz and green  
759 feldspar (and occasionally xenotime).

760

761 Table 2: Results from sample characterization. Alkaline mortars may have problems with late-in-  
762 formation pyrogenic carbonates. Abundant bright yellow-orange-red grains are a marker for  
763 limestone and marble that can carry geological carbonate. CL for sample J13-ESM-1 cannot rule  
764 out geological carbonate, because on non-luminescent limestone at Jerash (Lichtenberger et al.  
765 2015). The sample Kimito004Li was too small for alkalinity test.

766

767 Figure 3: Results from TGA for samples J13-ESM-1, TTK008, Kimito004Li, Kastel09, Kastel10  
768 and Merida003. Weight loss from TD of binder  $\text{CaCO}_3$  is seen from c. 640-770  $^\circ\text{C}$ . Pure calcite  
769 decomposing to calcium oxide has its normalized weight reduced from 1.0 to 0.56. A mortar sample  
770 may have a smaller reduction of normalized weight because of non-decomposable aggregates or  
771 hydraulic mortar minerals (Dodson 1990).

772

773 Figure 4: Calcite backgrounds for TD. The background correction is fitted:  $F^{14}\text{C}_{\text{Background}} =$   
774  $(0.19 \pm 0.6) \cdot 10^{-3} \text{ mgC} \cdot 1/\text{mass} + (3.2 \pm 0.3) \cdot 10^{-3}$ . A  $F^{14}\text{C}$  value of 0.0030 corresponds to a  
775 radiocarbon age of c. 46 600  $^{14}\text{C}$  years BP.

776

777 Figure 5: Radiocarbon profiles for TTK006, TTK005 and J13-ESM-1, see Table 1 for further  
778 information on sample aliquots. **A** TTK006 with TD and SQ, and TTK005 with SQ. The expected  
779  $F^{14}C$  values derive from the years 1300 AD and 1318 AD, and geological carbonate shifts many  
780 fractions to lower  $F^{14}C$  values. The weighted average of the 1<sup>st</sup> and 2<sup>nd</sup> fractions of TTK005 (SQ) is  
781  $F^{14}C=0.9277\pm 0.0029$ . SQ data taken from Lindroos et al. (2011; 2012). **B** J13-ESM-1 with TD and  
782 SQ. The charcoal sample J13-ESM-1C embedded in the mortar infers the expected  $F^{14}C$ , and  
783 geological carbonate shift many fractions to lower  $F^{14}C$  values. SQ data and charcoal data taken  
784 from Lichtenberger et al. (2015).

785

786 Figure 6: Radiocarbon profiles for Kastel09, Kastel10 and Kimito004Li, see Table 1 for further  
787 information on sample aliquots. **A** Kastel09 with TD and SQ, and Kastel10 with SQ. The expected  
788  $F^{14}C$  values derive from the years 1378 AD and 1388 AD. SQ data taken from Lindroos et al.  
789 (2020a). **B** The weighted average of the 1<sup>st</sup> and 2<sup>nd</sup> fractions of Kastel09 (TD) is  
790  $F^{14}C=0.9203\pm 0.0020$ , and this is calibrated (Bronk Ramsey 2009; Reimer et al. 2020). The first  
791 written source on Kastelholm is from 1388 AD. **C** TD and SQ for sample Kimito004Li. The  
792 expected  $F^{14}C$  values derive from the years 1400 AD and 1450 AD. **D** The weighted average of the  
793 1<sup>st</sup> and 2<sup>nd</sup> fractions of Kimito004Li (TD) is  $F^{14}C=0.9310\pm 0.0019$ , and this is calibrated (Bronk  
794 Ramsey 2009; Reimer et al. 2020). Kimito church's sacristy is from the 1<sup>st</sup> half of the 15<sup>th</sup> century.

795

796 Figure 7: Radiocarbon profiles for Merida003, see Table 1 for further information on sample  
797 aliquots. **A** TD and SQ profiles for sample Merida003. The expected  $F^{14}C$  values derives from the  
798 years 69 AD and 96 AD, the Flavian dynasty. Many fractions have higher  $F^{14}C$  values than

799 expected, probably because of alkalinity, delayed hardening or dolomitic chemistry. SQ data taken  
800 from Lindroos et al. (2020b). **B** SQ (repeated from 7A) and P+SQ profiles. More of the P+SQ  
801 profile is close to the expected  $F^{14}C$  value than the SQ profile, and preheating seems to remove  
802 some late-in-formation pyrogenic carbonates. The P+SQ profile is also published in Lindroos et al.  
803 (2020b).

804

805 Table 3: Summary of conclusiveness and accuracy of  $F^{14}C$  profiles in Figure 5-7. Conclusiveness is  
806 evaluated by criterion I, described in the discussion.